Feasibility Study of a Low Power Helicon Thruster

M. Manente[a], M.Walker[b], J. Carlsson[c], C. Bramanti[d] ,S.Rocca [e], D.Curreli[a], Y.Guçlu[a], D.Pavarin[a]

a) CISAS University of Padua Via Venezia 15 35131 Padova, Italy
b) Georgia Institute of Technology, Atlanta, GA
c) Txcorp Boulder Colorado USA
d) Advanced Concept Team ESA ESTEC
e) ONERA (Paris)

Abstract

Helicon thrusters have recently been considered as possible new electric propulsion (EP) systems thanks to the acceleration mechanism called the "current free double layer" which allows specific impulses up to 1300 s with argon and 4000 s with hydrogen. Although the primary interest of this technology was always regarding primary propulsion, this paper explores the possibility of using the helicon thruster as secondary propulsion system, e.g. station keeping or attitude control onboard satellites from mini to telecommunication class. Such a thruster provides several advantages with respect to EP systems currently in use: (i) consists of very few components, which increases reliability, (ii) thrust and power can be modulated, thus it is versatile, (iii) plasma interacts marginally with the thruster structure, thus erosion is not an issue, and (IV) is light and compact. Numerical analysis has been conducted through a combination of 1-D and 2-D numerical codes. A specific 1-D code named PPDL has been developed to simulate the potential drop acceleration. The main features of the code are: hybrid Boltzmann electron/drift-kinetic ion, inclusion of dominant 2-D effects, and high computational efficiency thorough an implicit non-linear Boltzmann solver. The 2-D code XOOPIC is freely available from the University of California, Berkeley. The limitations of XOOPIC are that no floating boundary condition can implemented on the electrostatic solver and a long computational time. To reduce computational time, the 1-D code is used to screen many different experimental conditions and to identify the correct boundary condition. The 2-D code is then used to refine the 1-D results. The two models, combined with a global model specifically developed to simulate the plasma behaviour inside the plasma source, have been run, through genetic algorithms to identify optimal thruster configurations in the 50-W power regime.

1. Introduction

Recently a strong interest in micro-propulsion has arisen within the space community: These devices will be required to deliver very low thrust values (millinewtons and below) and low impulse bits and should be characterized by engine masses and sizes smaller than current propulsion technology. Interest in such devices is driven by the needs of the most advanced missions currently being studied within the scientific space communities. Because a large fraction of launch costs consists of safety procedures surrounding the storage, handling, and loading of toxic and/or carcinogenic propellants used by established propulsion systems, additional cost savings can be obtained by utilizing environmentally safe propellants, with better performance and/or storage characteristics than existing monopropellants.

These needs involve primary propulsion and attitude control of micro-spacecraft having total wet masses around a few kilograms and precise positioning control of spacecraft constellation. Micropropulsion systems require miniature feed system components, such as valves, pressure regulators, flow controllers, and tanks. Thus, development of new propulsion hardware requires advanced microfabrication techniques, such as MEMS technology. Spacecraft with a mass less than 100 kg, but larger than a few tens of kilograms, may still be characterized by subsystem architectures that follow traditional design approaches to a large extent, in both component design and integration. To enable an order of magnitude reduction in spacecraft size while retaining mission capabilities, further developments in propulsion technology are needed.

Three classes of EP devices are currently in use or near being used in flight. These types are referred to as electrothermal, electrostatic, or electromagnetic devices, depending on the principle by which the working fluid is accelerated to provide thrust. Electrothermal thrusters create a high temperature fluid which provides a driving force by acceleration through a conventional nozzle. The thermal energy of the fluid is partly converted to kinetic energy. Electrostatic thrusters produce thrust by accelerating a charged plasma by means of a static electric field. Electromagnetic thrusters apply an electromagnetic field to accelerate an electrically charged plasma. This electromagnetic field can be self-induced or externally generated. The least complex EP system available is the resistojet. In a hydrazine resistojet, the heat of the products of hydrazine, decomposed in a catalyst bed, is resistively augmented in a heating coil. The increase in performance over monopropellants can range to 80 s, but this requires 0.3-0.4 kW of electrical power.

Hydrazine monopropellant thruster

Hydrazine monopropellant thrusters combine engine technology substantially simpler than that of bipropellant engine with high reliability, a relatively simple feed system. and intermediate performance characteristics (specific impulse (I_{sp}) is around 220 s for state-of-the-art hydrazine thruster technology). In a hydrazine thruster, the propellant is passed through a catalyst bed and decomposed. The decomposition products are nitrogen,

hydrogen, and ammonia. The catalyst pellets are contained within a mesh construction in a so-called catalyst bed. Upon contact with the iridium surfaces, the hydrazine decomposition reaction is initiated. Table 1 shows the performance of several hydrazine monopropellant thrusters.

	T [mN]	Isp [s]	mass [kg]	dimension [Ø mm]	m/T [kg/mN]
Primex MR 103	1	210	0,33	14,8x3,4	0,36667
Marquardt KMH S 10	1	226	0,33	14,6x3,2	0,36667
Daimler Chrysler	1	223	0,28		0,28
Primex MR-11E	2	213	0,33	16,9x3,8	0,15
Primex MR-111C	4	226	0,33	16,6x3,8	0,07416
Marquardt KMH S 17	4	230	0,38	20,3x3,2	0,08539
TRW MRE-1	5	220	0,82		0,164
TRW MRE-4	18	230	0,41		0,02278

Table 1: Performance of monopropellant hydrazine thruster

Cold gas thruster

Cold gas thrusters represent the smallest rocket engine technology available today. Cold gas systems are valued for their low system complexity, their small impulse bit, and the fact that, when using benign propellant (e.g. N_2) they present no spacecraft contamination problems. Cold gas systems are characterized by a low I_{sp}, unless very light gases (H_2, He) are used. Neither hydrogen nor helium is commonly used, however, since storage problem due to large and heavy tankage would result as a consequence of low gas density. Table 2 shows the performances of several cold gas thrusters.

	T [mN]	Isp [s]	Mass [kg]	m/T [kg/mN]
Moog A	5	65	0,0073	0,00163
Moog B	5	73	0,0055	0,00104
Moog C	289		0,0130	4,5E-05
Marotta	500	73	0,0500	0,0001

Table 2: Performance of cold gas thrusters

Arcjets

Low power arcjets perform well at 0.5 to 0.75 kW. Below 0.5 kW, the performance decreases. Current technology does not allow for operations at microspacecraft power levels.

Ion Thruster

The smallest ion thrusters available are the 10-cm diameter British DERA T5 and the DASA RITA thruster. A 13-cm diameter L-3 ETI XIPS thruster with an I_{sp} of 2585 s, overall efficiency of 51.3%, and power of 300 Watt was launched on the ASTRA 1G satellite on December 3rd, 1997. An experimental ion thruster was launched on-board the Japanese ETS-VI, but the spacecraft failed to reach its intended orbit and the test program was severely shortened. Ion thruster loss mechanisms, such as recombination, are dominated by wall effects. A reduction in the physical size will therefore reduce the efficiency and I_{sp}. Ion thrusters could be considered for microspacecraft propulsion if issues with wall losses, plume neutralization, and high-voltage arcing can be resolved. Table 3 shows the performances of small ion engines.

	T [mN]	P/T [W/mN]	Isp [s]	mass [kg]	m/T [kg/mN]	d/T [mm/mN]	efficiency
DERA T5	25	25	3110	1,7	0,068	4	0,6
DERA T8	150	26	3470	6,2	0,0413		0,65
RIT 10	10	44	3260	1	0,1		0,36
RIT 10 EVO	35	30	3700				0,67
RIT 25	25	32	3060	1,75	0,07		0,48
RIT 15PL	50	27	3600				0,67
RIT XT – Low Beam Voltage	100	24	3340				0,68
RIT XT – High Isp mode	150	33	5555				0,83
Laben Proel RMT	12	40	3600	1,6	0,1333	12,5	0,44
Hughes	18	25	2585	5	0,281	7,303	0,51
Hughes DS1 NSTAR	92	25	3280				0,64
JPL	31	29	3900	2,5	0,0807	4,839	0,66
NASA Lewis	11	28	2650			7,339	0,47
Keldysh Res center	6	27	3650			8,929	0,66
Keldysh Res center	19	26	3500			5,263	0,65

Table 3: Performance of ion thruster

Hall Thruster

The SPT-100 typically provides 80 mN thrust at an I_{sp} of 1600 s and 48% efficiency with an input power of 1.35 kW. A SPT-50 has been laboratory tested down to 0.09 kW with an I_{sp} of 700 s and efficiency of 21%. At the design point of 0.3 kW, the SPT-50 operates at an I_{sp} of 1160 s and an efficiency of 32%. Hall thruster scalability is critical. Table 4 shows typical Hall thruster performance.

	T [mN]	P/T [W/mN]	I_{sp} [s]	mass [kg]	m/T [kg/mN]	d/T [mm/mN]	Efficiency
Fakel SPT-100	90	16	1712	3,5	0,03889	1,11111	0,54
SPT-70	40	16	1510			1,75	0,46
Fakel SPT-60	30	17	1300			2	0,38
Fakel SPT-50	20	18	1250	0,9	0,045	2,5	0,35
Moskow SPT-30	13	20	1234	0,4	0,03077	2,30769	0,3
Fakel SPT-25	6,4	24	948			3,90625	0,19
T-27	9,6	21	1430				0,33
T-100	82,4	16	1573			1,21359	0,47
Keldysh X-40	35	15	1750			1,14286	0,56
Keldysh KM-37	18,4	16	1635				0,49
Keldysh KM-32	10,4	15	1410				0,45
SNECMA PPS 1350	85	18	1650	4,5	0,05294	1,17647	0,46
Busek BHT-HD-600	36	17	1700	2,2	0,06111	2,77778	0,5
Busek BHT-HD-1000	55,5	18	2051	3,5	0,06306	2,52252	0,56
Busek BHT-200-X2B	17	18	1600	0,9	0,05294	5,88235	0,45
Princeton	54,4	16	1550			1,65441	0,46
Un. of Hifa	39	17	1656			1,84615	0,49
D-38	11,4	19	1336				0,34
D-35	82	15	1263	4,35	0,05305	0,67073	0,4
Keldysh K-15	16	25	1718			0,9375	0,36

Table 4: Performance of Hall thrusters

Colloid Thruster

The Busek Corporation is developing a colloidal thruster system in the 25-μN class for the SBIR Air Force early warning satellite system. Stanford University is also involved in testing small colloid thrusters. Table 5 shows the performance of several colloidal thrusters.

	T [mN]	P[W]	P/T [W/mN]	Isp [s]	mass [kg]	m/T [kg/mN]	efficiency
Electro optical system	0,008	0,03	4,4	700	7,33	964,474	0,78
TRW	0,001	0,01	10,3	1450			0,69
TRW/Edwards AFB	0,159	1,4	8,8	1382			0,77
TRW/Edwards AFB	0,129	1,15	8,9	1405			0,77
TRW/Edwards AFB	0,335	2,41	7,2	1029	4,95	14,7982	0,7
Busek	0,189	6		400			
Stanford	0,001	0,01	10	500			0,25

Table 5: Performance of colloidal thrusters

Pulsed Plasma Thruster

Pulsed plasma thrusters (PPTs) are possibly the best candidate for many micro-propulsion tasks. Typical thrust levels are between 0.05 and 2 mN, I_{sp} about 1500 s, which makes this device well suited for accurate spacecraft positioning such as the multi-spacecraft interferometric experiment. The minimum impulse bits obtainable are on the order of 10 mN-s, with larger impulse bits possible up to 1 mN-s. A total impulse of up to 20 kN-s is targeted for larger systems. Performance does not significantly deteriorate with power level. Total impulse and impulse bit size can be varied by changing the fuel bar geometry. Space readiness has not been achieved. Table 6 shows the performances of typical PPTs.

	T [mN]	P[W]	P/T [W/mN]	I_{sp} [s]	mass [kg]	m/T [kg/mN]	efficiency
zond2	2,000			410	5	2,5	
LES 6	0,027	2,5	93	590			0,03
NOVA	0,370	30	81	850	7,1	19,1892	0,05
SMS	0,160	22	138	400			0,01
LES 8/9 (MIT)	0,600	25,5	43	1000	7,33	12,2167	0,12
Millipound	4,450	150	34	1210			0,18
PPT-4	0,450	15	33	1250			0,18
PPT-5	0,750	50	67	1750			0,13
OS-1	1,400	70	50	1400	4,95	3,53571	0,14
PPT	0,090	20	222		0,5	5,55556	
PPT	2,000	100	50	800			0,08
PPT	0,140	12,5	89	500			0,03
advPPT	4,200	133	32	515			0,08
APPT	5,200	250	48	1700			0,17

Table 6: Performance of PPTs

FEEP

Field emission electric propulsion (FEEP) has small thrust and high I_{sp}. Table 7 shows typical FEEP performance.

	T [mN]	P[W]	P/T [W/mN]	Isp [s]	m/T [kg/mN]	d/T [cm^3/mN]	efficiency
Alta FEEP-1000	1,200	72	60	10000	4,16667		0,82
Alta FEEP-100	0,120	7,2	60	10000			0,82
ARCS inFEEP-25	0,025			10000	284		
ARCS inFEEP-100	0,100			10000			
Centrospazio	0,040	2,7	66	9000	15	9600	0,65
Centrospazio	1,400	93	66	9000	0,85714	585	

Table 7: Performance of FEEP thrusters

2. Helicon thrusters

A helicon plasma thrusters is based on a helicon plasma [1] source specifically designed to produce high plasmas exhaust velocity. A helicon source is composed by very few physical elements:

- feeding system able to provide the required neutral gas flow
- glass tube where the plasma is generated

- an antenna having helix shape wrapped around the glass tube
- a system of coils placed coaxial with the glass tube to a magnetic field able to confine the plasma and to increase power deposition of the antenna

In this project the helicon source is used as the main element of the thruster. The thrust is obtained exhausting the plasma into vacuum driving it through a suitable magnetic field whose gradient is optimized to increase plasma velocity.

The thruster will implement one among the most advanced acceleration concept recently discovered: The potential drop which, under some circumstances, build-up on the exhaust zone. This phenomenon has been recently discovered at Australian National University [2-3] and called double layer. A numerical study conducted at CISAS under ESA contract has shown that this mechanism can provide reacceleration up to two times the ion Bohm velocity.[4]

3. Helicon thruster numerical models

The modeling approach here after proposed is based on three different numerical models: a) a global numerical model of the plasma source, b) a 1-D PIC code of the entire system, c) a 2-D PIC code of the entire system. The global model is used to simulate the plasma source behavior; it provides the source ionization rate, plasma density and electron temperature to the other two codes. A 1-D code named PPDL was developed specifically for this purpose. It is a hybrid code with Boltzmann electrons and drift-kinetic ions, inclusion of dominant 2-D effects and high computational efficiency through implicit nonlinear Boltzmann solver. The 2-D code used was XOOPIC, freely available from University of California, Berkeley. With XOOPIC it was necessary to perform fully electrostatic simulations with kinetic electrons, resulting in long computational times in order to analyze detachment features. A combined approach proved very useful where the 1-D code was used to rapidly screen many different experimental conditions and to identify the right boundary condition. The 2-D code was then used to refine the 1-D results.

3.1 Plasma source numerical model

A global model has been developed to better understand experimental observations and to lead the experiment design. This approach is similar to other global models previously developed for simulating process plasma sources.[9-14] The plasma balance equations for particles and energy are written for a uniformly distributed plasma inside of a region determined by the magnetic field configuration.

Many studies have investigated the plasma-neutral interactions, including the effect of neutral losses to ionization neutral heating.[15-21] Several models take into account the neutrals density by inserting source and sink terms into the neutral balance equation. These terms are related respectively to the flow rate from the reservoir and the flow rate to the vacuum pump.[15-20, 22-23] In other models the plasma-neutral interactions are not considered at all and no equations are written to follow the neutrals density behavior.[20-21] Due to the specific gasdynamic configuration of the device, the plasma-neutral interaction has been considered in this work by coupling a 0-D gasdynamic model of the entire system, with a global plasma model of the source. This model provides an estimate for the pop-off feeding-valve operation, efficiency of neutral pumping by the vacuum pump, and efficiency of a gas trap in the source to increase the ionization efficiency. The interactions that are taken into account in the model are:

- neutral density reduction due to ionization;
- neutral dissociation (molecular specie-atom species);
- zero dimensional gas dynamic analysis behavior in the plasma source and in the vacuum chamber; and
- wall recombination and volume recombination in the main vacuum chamber.

Plasma is generated in the source chamber. A preliminary investigation shows that in specific magnetic field configurations or in a specific operation mode (helicon mode), the plasmas could be confined inside of a volume smaller than the source chamber volume. The plasma is considered confined in a cylindrical volume, V_e with plasma radius r_p, and having the same length as the source chamber, L. Inside this volume different species are considered for every gas. The model follows the density of all of these species. Plasma also flows and diffuses through the external surfaces of the volume V_e. These surfaces are named in different way to highlight the different processes involved. The back axial surface is the surface in front of the feeding orifice. Plasma in this zone is electrostatically confined and the mass loss is calculated using Godyac and Maximov.[9] Plasma also diffuses through the radial surface, but in this zone the magnetic field generated by the solenoid coil improves the confinement. The particle loss in this area has been calculated with the Godyac and Maximov solution modified by Cheetham[9] to take into account the magnetic field contribution to the confinement. The axial surface toward the vacuum chamber is named the exhaust surface. Plasma flows in this zone with a speed that is a fraction of the ion sound velocity. The speed strongly depends on the shape of the plasma potential in this area. The calculation of this speed is beyond the purpose of this model. Thus, we introduce the cs coefficient into the numerical analysis to approximate the exhaust velocity. The exhaust velocity is the ion sound velocity multiplied by the cs coefficient that has been considered as a free parameter. This coefficient is evaluated using PIC codes.

Particles that diffuse through the lateral surface and through the back axial surface are neutralized. As will be explained later, the plasma equations are coupled with neutral equations since in the source chamber the neutral density is not constant, but free to change in relation to the neutral flow, the dissociation processes, and the plasma-neutral interaction. The reactions involving ionized species and electrons are found in literature. The particle balance equations for the ionized particles and electrons are written in a particle flux form, (particles/second m^3). The general form for the balance equations of charged particles is:

$$\frac{dn_i}{dt} = \Gamma_i^s - \Gamma_i^l - \Gamma_{Wi} - \Gamma_{EXH-i} \qquad (1)$$

Γ_i^s is for the *i*-species the source term due to plasma processes, Γ_i^L is the loss term due to plasma processes, Γ_{Wi} is for the *i*-species the loss term due to particle recombination at the wall (the particle diffuses through the wall sheath before reaching the wall), and Γ_{EXH} is the loss term due to the particle flow through the exhaust. The reaction rates are obtained by averaging the cross section for the specific reaction over a Maxwellian distribution.[10]

$$K_i = \left(\frac{m}{2\pi kT}\right)^{3/2} \int_0^\infty \sigma(v) v \exp\left(-\frac{mv^2}{2kT}\right) 4\pi v^2 dv \qquad (2)$$

In Equation 2 T is the electron temperature in eV and m is the particle mass, and σ is the cross section. Wall losses are calculated as in [15-22]. Ions lost at the exhaust are calculated as:

$$L_{EXH} = n_i \cdot u_B \cdot A_{EXH} \cdot cs$$
$$u_B = \sqrt{\frac{kT_e}{m_i}} \qquad (3)$$

In Equation 3 u_B is the Bohm ion velocity and A_{EXH} is the geometrical exhaust area.

At the exit of the plasma discharge section a variation in magnetic field could build-up a magnetic mirror, which would reflect part of the plasma flow. Therefore, the net flow is the difference between the incident flow and the reflected flow. The reflected flow depends on the magnetic field configuration and the plasma parameters as explained later in the section "Magnetic mirror".

To calculate the electron temperature, the power balance equation has been written as follows (units: W/m^3).

$$\frac{P_{ABS}}{Ve} = \frac{d}{dt}\left(\frac{3}{2} \cdot e \cdot n_e \cdot T_e\right) + \sum P_i + P_W + P_{EXH} \qquad (4)$$

P_{ABS} is the deposited power into the plasma that is assumed to be known, e is the electron charge, T_e is the electron temperature, and V_e is the plasma volume. P_i terms are the power lost in the *i*-reaction. The general formula is:

$$P_i = K_i \cdot E_{TH-i} \cdot n_e \cdot n_j \qquad (5)$$

where K_i is the rate constant for the specific reaction, E_{TH-i} the threshold energy for the *i*-reaction, n_e the electron density, n_j the density of the specie involved in the *i*-reaction. P_W is the power lost at the wall due to the electron-ion flow. P_{EXH} is the power loss associated with the electron and the ion flux at the exhaust, assuming that the escape velocity is the ion-Bohm velocity multiplied by cs. Experimental results [26] indicate the presence of a hot tail in the electron population in hydrogen and helium discharges. This distribution is modelled by adding two Maxwellian distributions: one with the temperature of the bulk of the plasma and one with the temperature of the hot tail. The model operates with argon, hydrogen or helium.

The numerical outputs of the model described above were compared with experimental data found in literature [5] about plasma parameters in the helicon stage. This operation made it possible to validate the model and to determine the value of few parameters. Figure 1 shows the comparison between the model results and experimental data found in literature.

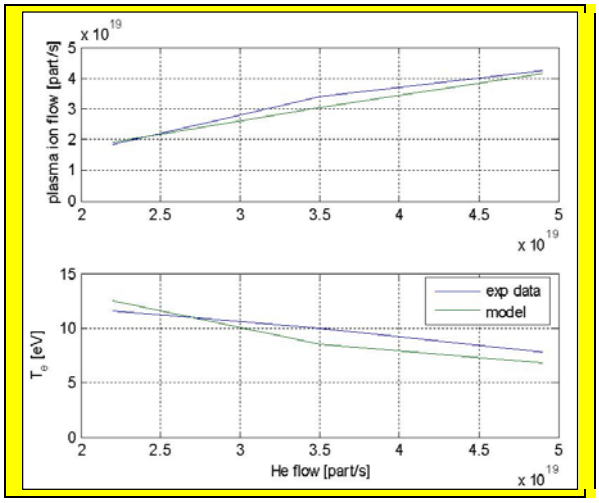

Figure 1: Comparison between experimental data and the numerical model. Helium discharge, 3 kW RF power

3.2 1-D PIC numerical model

PPDL[6, 26] is a modified version of an existing 1-D Particle-in-Cell (PIC) plasma model named PadPIC.[7] The main features of PPDL are:

- Drift-kinetic ions, where the magnetic moment is assumed to be an adiabatic invariant. The drift kinetic equation of motion
- The expansion of the magnetic field is considered
- Boltzmann electrons, assuming Maxwellian distribution and inertialess
- Floating boundary conditions
- Plasma generation is simulated through a source term

The advantage of Boltzmann electrons is that electron time scale (plasma and gyro periods) do not have to be resolved, but on the other side it requires a non-linear Poison solver to determine the electrostatic potential. With the hybrid Boltzmann electron/drift-kinetic ion approach, the time step is only limited by the ion period, which is two orders of magnitude larger than electron plasma period. The ion period can become very short in a strong magnetic field. Thus, PPDL is very fast, efficient, and still capable of simulating the relevant physics.

To better fit the experimental set-up the presence of magnetic field is simulated by the analytic solution of a field generated by one or more solenoids. The gradient of the magnetic field is also calculated analytically and used for adding the ∇B velocity to the drift-kinetic ions. The dilution of the charge density due to the expanding magnetic field is incorporated into the non-linear Poisson solver.

A plasma of radius r_0, density n_0, temperature T_e, and created in a uniform field B_0 is injected into a region of expanding field lines. The plasma is frozen to the field lines. The expansion of $B(z)$ and $n(z)$ plasmas along the magnetic field is also simulated using the relation:

$$\frac{n}{n_0} = \frac{B}{B_0} = \left(\frac{r_0(z)}{r(z)}\right)^2 \qquad (6)$$

where *r(z)* is the radius of magnetic lines at position *z*. PPDL can simulate the potential drop due to source and magnetic field configuration to accelerate the plasma after its creation.

PPDL is a monodimensional code developed to simulate the potential drop acceleration of ions in the helicon double layer thruster concepts, and it has been adapted to the simulation of this low-power thruster and considers both plasma source and acceleration. It performs a very fast simulation (due to Maxwellian electrons) of the entire system. In this way it is more suitable for the application inside a genetic algorithm to perform design optimization.

3.3 2-D PIC Simulations

Object-Oriented Particle-In-Cell (XOOPIC) is used to perform the simulations. XOOPIC is a 2D-3V relativistic electromagnetic open-source PIC code developed by the University of California, Berkeley. The object-oriented paradigm provides an opportunity for advanced PIC modeling, increased flexibility, extensibility, and efficiency.[8,27] XOOPIC includes a 2-D orthogonal grid: cartesian (x,y) or cylindrically symmetric (r,z) and moving window. It includes electrostatic and electromagnetic fields, and relativistic particles. The boundaries can be determined at runtime and include many models of emitters, collectors, wave boundary conditions and equipotentials. Because the dependence on the azimuthal angle is not expected to be relevant for double layer experiments, XOOPIC can be used as a 2-D r-z cylindrical PIC simulation. The code can handle an arbitrary number of species, particles, and boundaries. It also includes Monte Carlo collision algorithms for modeling collisions of charged particles with a variety of neutral background gasses. The same geometry and magnetic field configuration of PPDL was reproduced with XOOPIC to confirm and to refine the optimization results.

3.5 Thruster global design

The thruster has been designed with following strategy: The performance models described earlier are combined with a lumped structural model, which provides, (depending on the selected thruster configuration - mass flow rate, magnetic field, power, etc.), the total volume and mass.

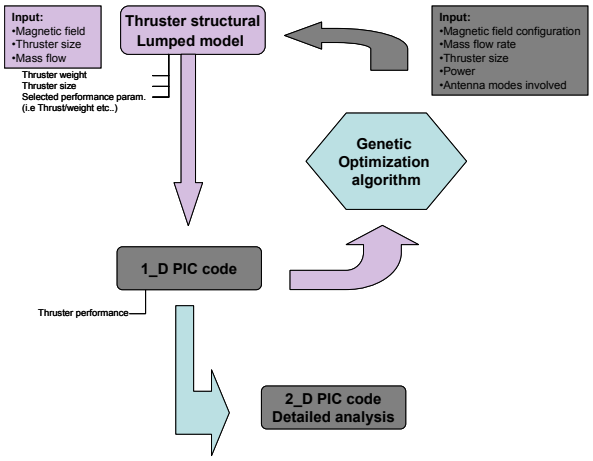

Figure 2: Optimization logic

A genetic algorithm is used to perform the optimization. The structure of the multi-objective evolutionary algorithm used in this work follows the main steps of a μ + μ evolution strategy. The evaluation steps include estimating the fitness functions from the actual decision variables and ranking the individuals according to the Pareto concepts. Then the Genetic Diversity Evaluation Method (GeDEM) is applied to establish a criterion for fitness assignment and to build the next population of parents. In short, the GeDEM preserves the genetic diversity of the best-so-far population of candidate solutions to the optimization problem by performing an additional evaluation after the common measure of objective fitness. This evaluation ranks the solutions according to their fitness value and their reciprocal distance as a way to give more reproduction chances to both highly-fit and highly-distant individuals. The loop starts again until the predetermined number of generations is reached.

This algorithm is used in order to identify the best thruster configuration as a trade off among performances, weight, and volume. The only thruster requirement is 50 W of available power. The thruster constraints are: a total mass lower than 1.6 kg and total volume lower than 1 dm^3.

First, the global model is used in combination with the structural model to identify the 10 most promising configurations. Second, these configurations are analyzed with the 1-D PIC model in order to identify the three best configurations, which are finally investigated with the 2-D PIC code in order to evaluate thrust and I_{sp}.

The gas used in simulations is argon. The reason is that it is much easier to be stored with respect to helium and hydrogen and provides a reasonably high I_{sp}.

The optimization variables are:

- source diameter
- mass flow rate
- magnetic field configuration

The ratio between source diameter and length is kept at 6.8 as an average value retrieved in literature. For each configuration the minimum value of the magnetic field is

assigned in order to allow a gyro radius equal to one-third of the source radius.

The total mass evaluation involves the estimation of the copper Helmholtz solenoids necessary to maintain the magnetic field line configuration required by the source and the potential drop for plasma acceleration.

The optimized thruster has the following features:

- Total mass (pressure reservoir excluded) 1.5 kg
- Magnetic field 150 G
- Total volume 0.8 dm^3
- Thrust 1mN
- I_{sp} 1350 s
- Power 50 W

The output values of optimization through the global source model and PPDL was confirmed by the simulation via XOOPIC which permits a better evaluation of thrust.

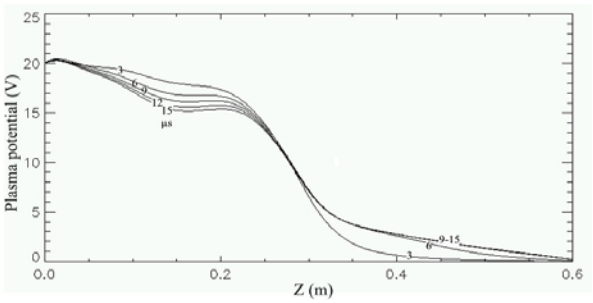

Figure 3: Axial plasma potentials for a conducting 20 V DC biased source upstream wall. The outer wall is a non-confining dielectric.

The thrust has been calculated with XOOPIC for four different detachment lines. Those lines are selected considering the axial positions from which the direction of the ion velocity approaches a constant. It is assumed that the distance from the helicon tube exit where the detachment takes place increases with the axial position. Therefore, the formula $T=\sum m*N*V_a*A$ is applied, iterated for every r_i along the supposed detachment line, where T is thrust, m is the ion mass, N is the density of ions inside the detachment cell at radius r_i, V_a is the average axial velocity inside the detachment cell, and A is the cross surface of the cell revolution along φ. Thus, for all the cells that follow the selected line, the ion density and average ion axial velocity is evaluated. The I_{sp} can be calculated by means of the formula $I_{sp}=(\sum N*V_a)/(\sum N*g)$, again iterated along the supposed detachment line, where g is the gravitational acceleration.

Table 8 shows a comparison between the designed helicon thruster and other propulsion systems.

		Ion Thruster type	Hall Thruster type	PPT type	Mini_helicon Plasma thruster
Thrust [mN}	mean	48,89	38,7	1,56	1
	min	5,6	6,4	0,027	
	max	150	90	5,2	
Specific Impulse[s]	mean	3484	1503	951,92	1350
	min	2585	948	400	
	max	5555	2051	1750	
Power [W]	mean	1363	646,9	67,73	30
	min	152	156	2,5	
	max	4922	1500	250	
Mass/Thrust [kg/mN]	mean	0,058	0,050	8,60	0,75
	min	0,179	0,031	2,50	
	max	0,041	0,063	19,19	
Power/Thrust [W/mN]	mean	29,4	17,47	75,38	30
	min	24	15	32	
	max	44	25	222	

		FEEP thruster type	Colloidal	Mini_helicon Plasma thruster
Thrust [mN}	mean	0,48	0,117	1
	min	0,025	0,00064	
	max	1,4	0,3345	
Specific Impulse [s]	mean	9666,67	980,86	1350
	min	9000	400	
	max	10000	1450	
Power [W]	mean	43,73	1,57	30
	min	2,7	0,009	
	max	93	6	
Mass/Thrust [kg/mN]	mean	76,01	52,37	0,75
	min	0,86	7734,375	
	max	284	21,91	
Power/Thrust [W/mN]	mean	63	8,27	30
	min	60	4,4	
	max	66	10,3	

Table 8: Comparison between the designed helicon thruster and other propulsion systems

Summary:

- The system presents a thrust lower than Hall thruster systems (SPT-70 - 40 mN, SNECMA PPS 1350 - 85 mN), but it uses less power and the mass and dimensions are significantly reduced compared to Hall thruster (their chamber diameter is around 50-100 mm or more), moreover the Hall thruster works at higher power.
- FEEPs have an I_{sp} (10,000 s) higher than HPH.com system, but the thrust is limited to 0.1-0.01 mN.

- PPTs (PPT-4, EOS-1) present similar characteristic (with a smaller thrust), but the mass is higher (up to 9 kg).

As a result, the following conclusions are drawn:

- The helicon based plasma thruster propulsion system in plasma configuration presents advantages with respect to other propulsion systems.
- The system presents a compact volume and low mass.
- The required electric power is very low (about 50 W).

3.6 Ongoing experimental activities

Based on the numerical results CISAS has designed an experiment to verify code results. The Georgia Institute of Technology (GA Tech) is conducting an extensive experimental characterization to verify effective thruster performances. Figure 4 shows a diagram of the experimental thruster.

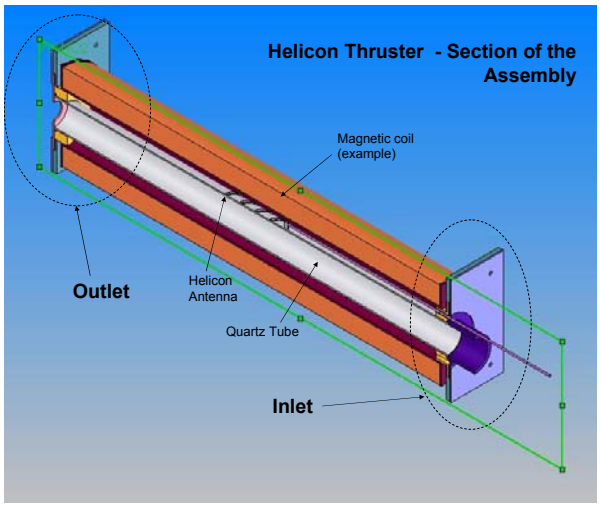

Figure 4: Diagram of the experimental helicon thruster.

GA Tech has the ability to operate the thruster over a forward RF power range of 50 W – 1.5 kW. Several different helicon antennas, and magnetic field configuration will be tested. All experiments are performed in GA Tech Vacuum Test Facility at an operating pressure less than $5x10^{-5}$ Torr. The thrust of the helicon thruster will be measured with a null-type inverted pendulum thrust stand. The ion exit velocity will be measured with a retarding potential analyzer. Moreover, CISAS will also conduct experimental tests in its own facility. The CISAS test results will be compared with results obtained at GA.

3.7 Conclusions

A mini helicon plasma thruster, has been designed at CISAS, to be mounted onboard a mini satellite for attitude and position control. The thruster has been designed to operate with 50 W of power. Thruster expected performances are 1 mN of thrust and 1350 s of I_{sp} with argon propellant. Moreover, the thruster is expected to weigh 1.5 kg and to have a volume of about 1 dm^3. Experimental analyses are currently ongoing in parallel at GA Tech and at CISAS.

Acknowledgment

The authors wish to thank Dr. Cinzia Giacomuzzo for her valuable work on the development of PPDL. This research has been partially supported by ESA-ARIADNA program.

Bibliography

1 - C. Charles, R.W. Boswell, P. Alexander, C. Costa, O. Sutherland, L. Pfitzner, R. Franzen, J. Kingwell, A. Parfitt, P.E. Frigot, J. Gonzalez del Amo, E. Gengembre, G. Saccoccia, R. Walker, "Helicon Double Layer Thrusters," 42nd AIAA/ASME/SAE/ASEE Joint Propulsion Conference & Exhibit, AIAA 2006-4844, 9 - 12 July 2006, Sacramento, California

2 - C. Charles, "Hydrogen ion beam generated by a current-free double- layer in a helicon plasma," Applied Physics Letters 84, 332-334, (2004).

3 - C. Charles and R.W. Boswell, "Current-free double-layer formation in a high-density helicon discharge," Applied Physics Letters 82, 1356 -1358, (2003).

4 - D. Pavarin, J. Carlsson, M. Manente, I. Musso, F. Angrilli, Numerical simulation of the Helicon Double Layer Thruster Concept, ESA Contract No. Ariadna 05/3201

5 – J. P. Squire, et al. "Experimental research progress toward the VASIMR engine," 29th International Electric Propulsion Conference, Toulouse, France, 2003.

6 - M. Manente, J. Carlsson, I. Musso, C. Bramanti, D. Pavarin, F. Angrilli, "Numerical simulation of the Helicon Double Layer Thruster Concept," 43rd AIAA/ASME/SAE/ASEE Joint Propulsion Conference & Exhibit, Cincinnati, AIAA 2007-5312, OH 8-11 July 2007.

7 – C. Birdsall, A. Langdon "Plasma Physics via computer simulation," Iop, Bristol, 1991.

8 - J. P. Verboncoeur, A.B. Langdon, N. T. Gladd, "An Object-Oriented Electromagnetic PIC Code," Comp. Phys. Comm., 87, May 11, 1995, pp. 199-211.

9- Cheetham A D, "Characterization and modeling of a helicon plasma source," J. Vac. Sci. Tech., A 16(5) Sep-Oct 1998.

10- Lieberman M A, "Global Model of pulse-power-modulate high-density, low-pressure discharges," Plasma Sources Sci. Tech. 5, (1996), 145-158.

11- C. Lee "Global Model of Plasma Chemistry in a High Density Oxygen Discharge," J. Electrochem. Soc, Vol. 141, No. 6, June 1994.

12- S. Ashida "Spatially averaged (Global) model of time Modulated High Density Chlorine Plasmas," J. Appl. Phys. Vol. 36, (1997), pp. 854-861.

13- S. Ashida, "Spatially averaged (global) model of time modulated high density argon plasmas," J. Vac .Sci. Tech., A 13(5), Sep/Oct 1995.

14- M. Meyyappan, "A spatially-averaged model for high density discharges," Vacuum, Vol. 47, N. 3, 215-220, 1996.

15- M. Mozetic "Atomic hydrogen density along continuously pumped glass tube," Vacuum, Vol. 5, N. 3-4, pp. 319-322, 1998.

16- G. R. Tynan, "Neutral depletion and transport mechanism in large-area high density plasma sources," Journal of Applied Physics, Vol. 86, N. 10, Nov 1999.

17- C. Lee "Global model of Ar, O2, Cl2, and Ar/O2 high-high density plasma discharges", J. Vac. Sci. Tech., A 13(2) Mar/Apr 1995.

18- T. Nakano “Ion and neutral temperature in electron cyclotron resonance plasma reactors”, Appl. Phys. Lett. 58(5), 1991, pp. 458-460.
19- J. Hopwood “Neutral gas temperature in a multipolar electron cyclotron resonance plasmas”, Appl. Phys. Lett. 58 (22), 3 Jun, 1991.
20- M. Meyyappan “A spatially-averaged model for high density discharges”, Vacuum, Vol. 47, N.3, 215-220, 1996.
21- B. Gordies, “Self-consistent kinetic model of low-pressure N2-H2 flowing discharges I-II,” Plasma Sources Sci. Tech. 7(1998), 378-388.
22- Suwon C, “A self consistent global model of neutral gas depletion in pulsed helicon plasmas”, Physics of Plasmas, Vol. 6, Jan 1996, pp. 359-365.
23- Gilland J, “Neutral Pumping in a Helicon Discharge”, Plasma Sources Sci. Tech., N. 7, 1998, pp 416-422.
24- Godyak V A, 1986 S.
25- M. I. Panevsky “Characterization of the Resonant Electromagnetic Mode in Helicon Discharges” Ph.D. Thesis, University of Texas at Austin, 2003.
26- Manente M., Musso I., Carlsson J., Giacomuzzo C., Bramanti C., Pavarin D. “1D-simulation of helicon double layer thruster” 30th International Electric Propulsion Meeting Florence, Italy - September 17-20, 2007.
27- Musso I., Manente M., Carlsson J., Giacomuzzo C., Bramanti C., Pavarin D. “2D-OOPIC Simulations of the Helicon Double Layer” 30th International Electric Propulsion Meeting, Florence, Italy - September 17-20, 2007.